

# Intrinsic geometry approach to surface kinetic roughening

Javier Rodríguez-Laguna<sup>1,3,\*</sup>, Silvia N. Santalla<sup>2</sup>, and Rodolfo Cuerno<sup>1</sup>

<sup>1</sup>*Mathematics Department and Grupo Interdisciplinar de Sistemas Complejos (GISC),*

*Universidad Carlos III de Madrid, Leganés (Madrid), Spain*

<sup>2</sup>*Physics Department, Universidad Carlos III de Madrid, Leganés (Madrid), Spain*

<sup>3</sup>*ICFO–Institute of Photonic Sciences, Castelldefels (Barcelona), Spain*

(Dated: April 1, 2011)

## Abstract

A model for kinetic roughening of one-dimensional interfaces is presented within an intrinsic geometry framework that is free from the standard small-slope and no-overhang approximations. The model is meant to probe the consequences of the latter on the Kardar-Parisi-Zhang (KPZ) description of non-conserved, irreversible growth. Thus, growth always occurs along the local normal direction to the interface, with a rate that is subject to fluctuations and depends on the local curvature. Adaptive numerical techniques have been designed that are specially suited to the study of fractal morphologies and can support interfaces with large slopes and overhangs. Interface self-intersections are detected, and the ensuing cavities removed. After appropriate generalization of observables such as the global and local surface roughness functions, the interface scaling is seen in our simulations to be of the Family-Vicsek type for arbitrary curvature dependence of the growth rate, KPZ scaling appearing for large systems sizes and sufficiently large noise amplitudes.

PACS numbers: 68.35.Ct, 05.10.Gg, 64.60.Ht, 81.15.-z

---

\* jrlaguna@math.uc3m.es

## I. INTRODUCTION

Kinetic roughening in non-equilibrium interfacial growth has been investigated for a long time both as a fundamental problem in statistical mechanics and as a model to relevant physical systems, such as dynamics of thin films, fluid flow, flame front propagation, or undifferentiated biological growth [1]. Starting from a flat shape, for many interfaces it is generally observed that they roughen until eventually a steady state is attained, in which the interface roughness,  $W$  (root-mean-square deviation around the mean interface position) scales in a nontrivial way with the system size  $L$ , as  $W \sim L^\alpha$ , where  $\alpha$  is the so-called roughness exponent. At short times in these systems, the roughness scales as a power law of time,  $W(t) \sim t^\beta$ , with  $\beta$  being called the growth exponent [1]. The saturation roughness can be measured at smaller length scales  $l$  than the system size, another power law ensuing,  $W(l) \sim l^{\alpha_{\text{loc}}}$ . If the local and global roughness exponents are equal,  $\alpha_{\text{loc}} = \alpha$ , the system follows the so-called Family-Vicsek (FV) Ansatz, that is a generalization of that expected for equilibrium critical dynamics [1]; otherwise, *anomalous scaling* occurs [2, 3] in which interface fluctuations follow different laws at small and large scales, a fact that is not uncommon when the interface profile displays many large jumps and high slope values [4, 5]. In general, the values of the critical exponents  $\alpha$ ,  $\alpha_{\text{loc}}$ , and  $\beta$  identify universality classes that play an important role in the classification of nonequilibrium processes in spatially extended systems [6].

Fluctuations arise in the above physical systems due to a variety of sources, such as non-homogeneous driving, randomness of growth events, etc. Dynamically, and in the absence of specific conservation laws that constrain the evolution of the interface [2], they compete with irreversible growth, that can be simply represented by a constant growth rate along the local normal direction to the interface, and are attenuated through various relaxation processes. The latter can be differential absorption due to curvature effects (e.g., condensation of atoms from a vapor phase is more effective at surface valleys of a solid than at surface peaks) [7], to surface diffusion (atoms move from peaks to valleys) [8–10], etc. Different relaxation mechanisms can give rise to different universality classes, some of which may in general appear as transients during the system evolution.

One of the most fruitful approaches to surface kinetic roughening is the study of stochastic partial differential equations (SPDE) of a certain *height function*,  $h(\mathbf{x}, t)$ , that represents the

surface height position at time  $t$  above point  $\mathbf{x}$  on a reference plane, in the so-called *Monge gauge* [11, 12]. This implies the assumption that the interface has no *overhangs*. Moreover, most height equations in this context rely on a *small-slope* approximation that allows to strongly simplify the analytical formulation. However, this simplification may be at the cost of inaccuracies in the physical description. For instance, surface diffusion is thus taken along the horizontal substrate plane (instead of along the interface) and is severely overestimated in regions of high slopes, giving rise to large *grooves* as in the so-called linear Molecular Beam Epitaxy (MBE) equation [13].

The very same Kardar-Parisi-Zhang (KPZ) equation [7], that is one of the most important SPDEs within the study of kinetic roughening—and within non-equilibrium statistical mechanics indeed—, was actually formulated within both the no-overhang and the small slope approximations. The fact that the corresponding roughness exponent  $\alpha_{\text{KPZ}} < 1$  [1] makes this approximation self-consistent, in the sense that slopes remain small on average. Nevertheless, the derivation of this equation being based on rather general considerations, a natural question arises as to what is the effect of relaxing these approximations. Actually, early reports [14] already claimed that relaxing the no-overhang approximation in a KPZ-type equation leads to a larger value for the growth exponent than that characteristic of the standard KPZ equation, although no information was provided on the value of the roughness exponent, nor later confirmations of this result are available. One of the motivations of the present work is to address a more systematic study along these lines. The question becomes all the more interesting since experimental realizations of KPZ scaling are remarkably scarce, in spite of the wide asymptotic universality that it is expected to have on theoretical grounds [15, 16]. Nevertheless, this universality class has been indeed verified in experiments very recently [17], including detailed predictions [18] on the asymptotic height distribution for the case of growth in a circular geometry. Analogous predictions are also available for the simpler case of a *band geometry* [19] in which boundary conditions are periodic or free, and the initial interface is a straight, horizontal line. Still, these remain to be experimentally assessed [17].

Actually, the relation between the scaling properties of a given SPDE in band and in circular geometries has been the focus of a recent controversy that has arisen from conflicting analytical predictions [20–22]. These unavoidably require approximations, since even equations that are linear in a band geometry become nonlinear in the circular setting. Thus, in

order to address the issue, it would be interesting to be able to study numerically the same SPDE in both cases. The circular geometry requires naturally a multiple valued interface (as seen from a Monge gauge) and arbitrary interface orientations, the additional existence of overhangs being again the more complete situation to be considered. This constitutes a second motivation for the present work, and makes the formulation of such an equation in a band geometry —as in the seminal formulation by KPZ— a natural preliminary step. Note, moreover, that the observables (correlation functions, etc.) also need to be adapted to the type of geometry in which the continuum model is formulated, see e.g. [23] and references therein. Again from this point of view, starting out with the band geometry seems a natural choice.

Previous attempts have been made in order to study continuum models of kinetic roughening beyond the two approximations mentioned. For instance, Siegert and Plischke [24], Maritan *et al.* [14] or Family and Amar [13] considered various relaxation operators still in the Monge gauge, but beyond the small slopes approximation, thus studying very complex and highly nonlinear SPDEs that are hard to deal with even numerically. Actually, later developments have questioned the reliability of the schemes employed, since the standard finite difference discretization of nonlinear terms has been shown to lead to numerical inaccuracies and instabilities (see an overview in e.g. [25]). Approximations in the corresponding SPDEs are also usually performed in the study of continuum growth equations in circular geometry, typically including the neglect of overhangs as well as additional simplifications, see e.g. [23, 26] and references therein. The specific case of the KPZ equation has been addressed in some of these works [14, 23] and elsewhere, see e.g. [27, 28], although overhangs seem to have been consistently neglected in all these SPDE-based approaches.

Also, phase-field studies have been carried out since the pioneering work of Kéblinski *et al.* [29, 30]. However, while in this class of studies arbitrary interface geometries are available, computational expense is sufficiently high that, to our knowledge, no complete systematic study of scaling properties is available so far. Moreover, connection with the KPZ equation is at best indirect via the asymptotic behavior, if appropriate.

In this work, our approach is to study a one-dimensional interface as a 2D curve in a band geometry as described above, that evolves under a continuum equation whose terms are determined by its intrinsic geometry. Actually, these are the same as those that led to the formulation of the KPZ equation, but now free from the no-overhang and the small-

slope approximations. We study the ensuing model numerically, carrying out simulations with an adaptive number of points, and doing measurements in a geometrically natural way. The equations do not distinguish between the horizontal (substrate) and vertical (growth) directions, their difference residing only in the initial and boundary conditions.

The paper is organized as follows. Section II introduces the physical model we study and its geometric interpretation. Next, in Section III, we discuss the numerical implementation of the simulations. In Section IV the observables to be measured are considered, while results are presented in Section V. Further discussion of these is presented in the final Section VI, together with some conclusions and indications of potential new directions for future work.

## II. INTRINSIC GEOMETRY FOR SURFACE GROWTH IN 1D

### A. Intrinsic Geometric Preliminaries

Our 1D interface is given mathematically by a curve  $\gamma$  in a 2D band geometry, that we take to be an infinite cylinder of circumference  $L$ , i.e.,  $\underline{r} : [0, 1] \mapsto S^1 \times \mathbb{R}$ . Of course,  $\underline{r}(0) = \underline{r}(1)$ . The curve is assumed to wrap around the cylinder exactly once, thus separating a *solid phase* (below) from a *dilute phase* (above).

At any point on the curve  $\underline{r}$ , let us consider the unitary tangent vector field,  $\underline{u}_t$ , and the normal vector field pointing towards the dilute phase,  $\underline{u}_n$ . The curvature  $K(\underline{r})$  *along* the interface will be given by the inverse of the radius of the best fitting (osculating) circle.

For any scalar field defined on the curve  $\phi(\underline{r})$ , we define its  $\gamma$ -gradient as the derivative *along* the curve, parametrized by its arc-length  $s$ , pointing along the tangent:

$$\nabla_\gamma \phi(\underline{r}(s)) = \frac{\partial \phi(\underline{r}(s))}{\partial s} \underline{u}_t(\underline{r}(s)). \quad (1)$$

The *divergence* along the curve of such vector field allows us to define a Laplace-Beltrami operator as

$$\nabla_\gamma^2 \phi(\underline{r}(s)) = \frac{\partial^2 \phi(\underline{r}(s))}{\partial s^2}. \quad (2)$$

### B. Physical Model

In order to have a physical image in mind, let us consider a system in which atoms are interchanged between a dilute (vapor or liquid) and a solid (aggregated) phase, in such a

way that the latter grows at the expense of the former, as in the production of thin films [15]. We will consider absorption and desorption to be non-directional phenomena, and the possibility of atomic diffusion at the interface. The chemical potential difference at an interface point,  $\mu(\underline{\mathbf{r}})$ , will be the only driving force for growth. On the solid side of the interface (subindex  $s$ ), the chemical potential will be given by [2]

$$\mu_s(\underline{\mathbf{r}}) = \mu_{s,0} - \mu_{s,1}K(\underline{\mathbf{r}}), \quad (3)$$

where  $\mu_{s,0}$  and  $\mu_{s,1} > 0$  are empirical parameters, and the local curvature  $K(\underline{\mathbf{r}})$  provides a measure of the number of local “dangling bonds”. We will consider  $K$  to be positive when the interface is concave as seen from the dilute phase. On the other hand, the chemical potential in the dilute (“vapor”, subindex  $v$ ) phase is  $\mu_v(\mathbf{r}) = \mu_{v,0}$ . Given that the solid phase is growing at the expense of the dilute phase, we can take  $\mu_{s,0} < 0$  and  $\mu_{v,0} = 0$  without loss of generality [2]. On the other hand, particles may move along the surface in their attempt to minimize their chemical potential. This process is called *surface diffusion* [31, 32]. Locally, the particle current will be proportional to the *surface gradient* of  $\mu_s$ ,

$$\underline{\mathbf{j}}_s(\underline{\mathbf{r}}) \propto -\nabla_\gamma \mu_s(\underline{\mathbf{r}}). \quad (4)$$

Conservation of the number of particles requires that they aggregate to the solid phase at a rate proportional to the divergence of this current [2], thus

$$\nabla_\gamma \cdot \underline{\mathbf{j}}_s(\underline{\mathbf{r}}) \propto -\nabla_\gamma^2 \mu_s(\underline{\mathbf{r}}) = \mu_{s,1} \nabla_\gamma^2 K(\underline{\mathbf{r}}). \quad (5)$$

In line with the seminal approach by KPZ [7], a point at the interface  $\underline{\mathbf{r}}$  is assumed to move along the local normal direction, with a velocity that is proportional to the rate at which particles accumulate there, namely,

$$\partial_t \underline{\mathbf{r}} = \left( -\Gamma(\mu_s(\underline{\mathbf{r}}) - \mu_v) - \nabla_\gamma \cdot \underline{\mathbf{j}}_s(\underline{\mathbf{r}}) + \eta_v(\underline{\mathbf{r}}, t) \right) \underline{\mathbf{u}}_n, \quad (6)$$

where  $\Gamma > 0$  is a mobility constant [2] and  $\eta_v$  is a zero-average noise term —describing, e.g., fluctuations in the rate of growth events— that we will take as Gaussian, with zero average, and white both in space and time,

$$\langle \eta_v(\underline{\mathbf{r}}, t) \eta_v(\underline{\mathbf{r}}', t') \rangle \propto \delta(\underline{\mathbf{r}} - \underline{\mathbf{r}}') \delta(t - t'). \quad (7)$$

Note that the delta function in (7) is evaluated at points *on* the interface. Thus, it does not correspond to a delta function on the horizontal substrate plane.

The general form of the ensuing evolution equation is thus

$$\partial_t \mathbf{r} = (A_0 + A_1 K(\mathbf{r}) - A_2 \nabla_\gamma^2 K(\mathbf{r}) + A_n \eta(\mathbf{r}, t)) \mathbf{u}_n. \quad (8)$$

This equation contains four terms:

- A constant term,  $A_0$ , measuring the average difference between the chemical potentials in the dilute and solid phases.
- A term proportional to the curvature, with coefficient  $A_1 > 0$ , having the physical interpretation of surface tension [2].
- A term proportional to the Laplacian of the curvature field along the curve, with coefficient  $A_2 > 0$ .
- A white noise term, due to the fluctuations in growth events, with variance  $A_n^2$ .

In this work we study the scaling properties of Eq. (8) for  $A_2 = 0$ , leaving the general case for further work. Therefore, the equation under study will be

$$\partial_t \mathbf{r} = (A_0 + A_1 K(\mathbf{r}) + A_n \eta(\mathbf{r}, t)) \mathbf{u}_n. \quad (9)$$

This SPDE is analogous to the KPZ equation in the sense that it incorporates the same basic ingredients, namely, growth along the local normal direction, relaxation by surface tension, and fluctuations, but there are several important differences: (a) growth is always normal to the interface, while in the KPZ equation this condition holds only approximately; (b) we employ the full curvature, which is nonlinear if written in the Monge gauge, and (c) noise is normal to the interface, which means that, as seen in the Monge gauge, it is *multiplicative* and *correlated*.

In order to represent an interface, the curve should be *simple* for all times, i.e.: no multiple points are allowed. Therefore, Eq. (9) should be *supplemented* with a condition regarding the treatment of self-intersections. Our criterion is simply *removal*, keeping the component which wraps around the cylinder.

Finally, an initial condition is required. Unless otherwise specified, the interface will start as a horizontal line.

### III. NUMERICAL SIMULATIONS

The numerical discretization of Eq. (9) has been carried out keeping in mind the desideratum of *geometric naturality*, using concepts borrowed from *discrete differential form* theory [33]. The idea of our numerical procedure is to employ an adaptive scheme that does not particularly privilege any system direction, and that avoids e.g. standard explicit finite differences discretization of the various differential operators appearing, since this requires an explicit parametrization of the interface and is prone in this context to numerical instabilities, see e.g. [34] and references therein. The guiding physical principle is to use discrete counterparts of the operators appearing in Eq. (9), which are geometrically motivated.

The interface is simulated numerically by a chain of points  $\{P_1, \dots, P_N\}$ , with adaptive  $N$  and periodic boundary conditions,  $P_{N+1} = P_1$ . It is implemented in the computer in the form of a *linked list*, ensuring easy insertion and deletion of points. This set fulfills the following *continuity condition* [35]: the distance between any couple of neighboring points should always be in the interval  $[l_{min}, l_{max}]$ . Let us use the symbol  $d_{i,j}$  for the distance between any two points of the set. Then, at every time step, this condition is ensured using the following algorithm for every couple of nearest neighbors  $P_i, P_{i+1}$ :

- If  $d_{i,i+1} < l_{min}$ , remove  $P_{i+1}$  from the list.
- If  $d_{i,i+1} > l_{max}$ , add a new point  $P_{i+1} = (P_i + P_{i+1})/2$  (and shift the indices appropriately).

Application of this algorithm ensures that the representation of the interface is homogeneous. It is important, in all simulations, to generate the initial points randomly, in order to avoid lattice artifacts.

Next we provide a discrete approximation to the different geometric fields needed to simulate Eq. (9). The tangent vector field,  $\underline{u}_t(x)$  is approximated by  $(\underline{u}_t)_{i,i+1} \approx (P_{i+1} - P_i)/d_{i,i+1}$ . Notice that these values are not attached to single points, but to *links* between two consecutive points. With it we can approximate the normal vector field,  $(\underline{u}_n)_{i,i+1}$ , finding the orthogonal vector to  $(\underline{u}_t)_{i,i+1}$ , pointing towards the dilute phase.

The curvature field,  $K(\mathbf{r})$ , is approximated using the triangle  $P_{i-1}, P_i, P_{i+1}$ . We define  $K(P_i)$  as the inverse of the radius of the circumscribed circle passing through all three points.



Let  $\alpha_i$  be the angle at  $P_i$ . Then,

$$K_i \equiv K(P_i) \approx \frac{2 \sin(\alpha_i)}{d_{i-1,i+1}}. \quad (10)$$

Notice that, as defined, the sign of the curvature depends on the sign of  $\alpha_i$ . As in the previous Section, it will be positive when the interface is concave, as seen from the dilute phase.

As our last step, we will determine the approximation to the gradient and Laplacian along the curve of any scalar field  $\phi(\mathbf{r})$ , using the notation  $\phi_i \equiv \phi(P_i)$ ,

$$(\nabla_\gamma \phi)_{i,i+1} \approx \frac{\phi_{i+1} - \phi_i}{d_{i,i+1}} (\mathbf{u}_t)_{i,i+1}. \quad (11)$$

These values are attached to links, not to points. The approximation to the Laplace-Beltrami operator is computed as the (numerical) divergence of that expression:

$$(\nabla_\gamma^2 \phi)_i \approx \frac{2}{d_{i-1,i} + d_{i,i+1}} \left( \frac{\phi_{i+1} - \phi_i}{d_{i,i+1}} - \frac{\phi_i - \phi_{i-1}}{d_{i-1,i}} \right). \quad (12)$$

This formula may be formally justified using the notion of Hodge dual [33].

As pointed out before, the interface may tend to create *self-intersections*, leading to cavity formation. Our code detects such self-intersections and removes one component, keeping the one which wraps around the cylinder. The detection algorithm is one of the most delicate and costly ingredients of our numerical scheme.

Finally, concerning the time evolution, the SPDE (9) is simulated using the usual Euler-Maruyama algorithm. We have ensured that our  $\Delta t$  is small enough for the computations by repeating a selection of them with smaller values, always obtaining convergence. Regarding the noise amplitude, it is important to remark that, in the discretized SPDE, it must be multiplied by  $(\Delta s)^{-1/2}$ , where  $\Delta s$  is the arc-length interval corresponding to each point. This guarantees that the noise amplitude does not depend on the local interface orientation [12].

Additional checks have been performed on our algorithm in order to reproduce expected features in the behavior of Eq. (9) (not shown): (1) In the deterministic case ( $A_n = 0$ ) with  $A_0 = 0$ , we have performed a linear stability analysis of Eq. (9), plotting the relaxation time of a sinusoidal initial condition with wave-vector  $k$ , obtaining the expected diffusion-like relation between typical relaxation time and spatial frequency,  $\tau \sim k^{-2}$ . In this sense, the deterministic case of Eq. (9) reproduces (non-linear) diffusion. (2) For small non-zero  $A_0$ ,

with  $A_n = A_1 = 0$ , a sinusoidal perturbation evolves towards the typical deterministic KPZ arcade.

#### IV. MEASUREMENTS

The standard basic observable in kinetic roughening theory is the global interface *width* or surface roughness. It is usually defined within the Monge gauge as

$$W_{\text{Monge}} = \left\langle \overline{(h - \bar{h})^2} \right\rangle^{1/2}, \quad (13)$$

where  $h$  is the height of the interface, as measured from a horizontal reference line,  $\bar{\phantom{x}}$  stands for space average across the full system and brackets denote noise realizations. This definition, therefore, privileges the horizontal orientation. Moreover, if the interface presents *overhangs*, the very use of  $h(x)$  becomes ambiguous.

In many applications and in experimental studies of e.g. thin film dynamics [36], it is customary to *remove the plane*, i.e., finding the optimal orientation which can be taken as the horizontal. Our definition of interface width goes beyond this, being completely *intrinsic* at every length scale. Given any portion of interface, proceed in the following way:

- Find the straight line which makes the best fit to the curve.
- Compute the root mean square distance of the interface points to this line.

Skipping the first step and considering the best fitting line to be horizontal amounts to using the Monge gauge definition of interface width. Note that the fit is *not* an usual least-squares fit. In such a case, the minimized distances are taken along vertical lines. In our case, we minimize the actual distances, i.e., along a *diagonal* line, from the curve points to the fitting line.

Likewise, we define local width  $w(l, t)$  at any length scale  $l$  in the usual way: sample the surface using *windows* of size  $l$ , and measure the average width obtained, following the previous procedure. Of course, it is expected that  $w$  should be an increasing function of  $l$ . At the maximum length-scale,  $l = L$ , we retrieve the global width  $W(t) = w(L, t)$ . We should remark that the windows should be *random*. Otherwise, lattice artifacts are bound to appear.

The Monge-gauge roughness at small scales,  $\lim_{l \rightarrow 0} w_{\text{Monge}}(l, t)$ , describes the *slopes statistics*. In our case, if the surface is smooth below a certain cutoff length, such limit will be close to zero. If the interface is defined, as in our numerical simulations, by a set of linked line segments whose lengths lie in a certain interval, there is an upper bound for the roughness at each scale.

A power-law behavior is expected,  $w \sim l^{\alpha_{\text{loc}}}$ , for length scales under a certain correlation length,  $l < \xi(t)$ . Length scales above this value are still uncorrelated. As time evolves,  $\xi(t)$  increases until it reaches the system size. At that time all length scales are correlated, the system saturates to a stationary state and its width does not increase any further. The correlation length grows with another power law,  $\xi(t) \sim t^{1/z}$ , defining the *dynamic exponent*,  $z$ . Using this definition, it is easy to check that the *saturation time* scales as  $t_s \sim L^z$  [1]. Scaling is *regular*, or FV type, when the roughness of the correlated scales stays fixed for all times. In that case,  $\alpha_{\text{loc}} = \alpha$  and it can be shown that  $z = \alpha/\beta$  [1]. On the other hand, in the presence of anomalous scaling,  $\alpha_{\text{loc}} \neq \alpha$  and the roughness of the correlated scales keeps increasing after correlation, only saturating when  $\xi(t) = L$  [2, 3].

## V. RESULTS

Our main result is that, in spite of indeed featuring overhangs and relatively large local orientation angles, interfaces described by Eq. (9) follow a standard Family-Vicsek scaling, with exponents that fit into the standard universality classes. For smaller systems or low values of  $A_n$ , we obtain exponent values that are not far from those of the Edwards-Wilkinson (EW) universality class in 1D, i.e.,  $\alpha_{\text{EW}} = \alpha_{\text{EW},\text{loc}} = 1/2$ ,  $\beta_{\text{EW}} = 1/4$ ,  $z_{\text{EW}} = 2$ . This is the behavior associated with the weak coupling regime of the KPZ equation. Indeed, recall that in the Monge gauge the (naive) KPZ coupling constant scales as the square of the noise amplitude [1]. If  $L$  and  $A_n$  are large enough, and within error bars, we obtain exponent values compatible with those of the (strong coupling) 1D Kardar-Parisi-Zhang universality class, namely,  $\alpha_{\text{KPZ}} = \alpha_{\text{KPZ},\text{loc}} = 1/2$ ,  $\beta_{\text{KPZ}} = 1/3$ ,  $z_{\text{KPZ}} = 3/2$ . It is also remarkable that  $A_0$  plays no role in the determination of the universality class.

The system size of the simulations span a wide range of length scales, from  $L = 0.5$  to  $L = 500$ , always ensuring that the continuum limit has been achieved. For the largest sizes, where KPZ scaling is found, we have used  $\Delta t = 5 \cdot 10^{-3}$ , and spatial cutoffs  $l_{\text{min}} = 5 \cdot 10^{-5}L$

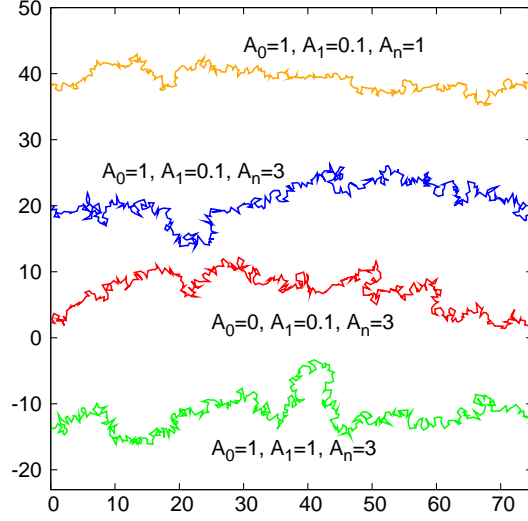


FIG. 1. Typical interface profiles for  $L = 75$  at saturation ( $t = 3000$ ) for different values of the parameters as indicated. The curves have been artificially offset in the vertical direction in order to allow comparison. All units are arbitrary.

and  $l_{max} = 5 \cdot 10^{-3}L$ . With these values, the number of points composing our simulated interfaces range typically between  $100 \lesssim N \lesssim 1000$ . Simulation times have reached  $t = 7000$  in order to ensure saturation to a steady state. Equation parameters have been taken of order unity:  $A_0 \in [0, 1]$ ,  $A_1 \in [0, 1]$  and  $A_n \in [0, 3]$ . Ensemble convergence is ensured by taking, in most cases, 200 samples or more.

Roughness measurements are done using our diagonal-fitting algorithm, although checks have been performed with the usual Monge-gauge definition, with no change in the exponents. We should remark that the simulation algorithm is extremely robust and does not suffer from instabilities.

Fig. 1 shows three typical interface profiles for  $L = 75$ , for the same times ( $t = 3000$ ), once saturation is achieved, for different values of the parameters. Note the relatively large slope values and the presence of overhangs. As intuitively expected, comparison between the orange and the pink curves illustrates the increased abundance of overhangs for larger noise intensities. However, changing from the latter to the red interface, we are led to expecting little influence of the value of  $A_0$  on the morphological properties. In turn, the green line corresponds to a parameter condition that differs from that of the red line in the value of  $A_1$ . As seen in Fig. 2, this also has little effect in the scaling behavior.

The time evolution of the global interface width is shown in the left panel of Fig. 2 from

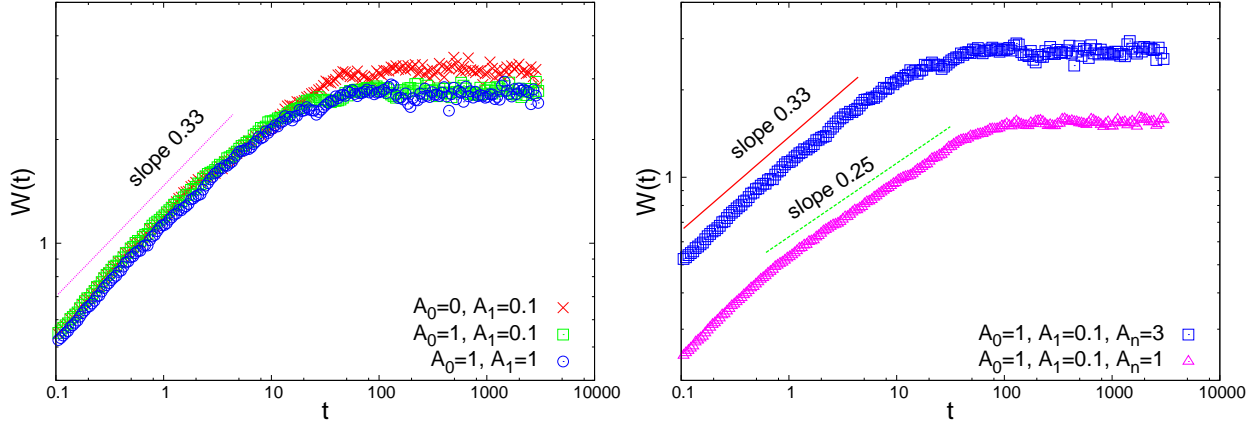


FIG. 2. Time evolution of the global interface width for  $L = 75$  and different parameter choices. Left panel: for  $A_n = 3$ , the scaling behavior does not depend appreciably on the values of  $A_0$  and  $A_1$ . The straight line is a fit to the data within the corresponding time interval, its slope being close to the KPZ behavior  $\beta_{\text{KPZ}} = 1/3$ . Right panel: comparison between  $A_n = 3$  case shown in the left panel and  $A_n = 1$ . The straight lines are obtained from fits to the data within the corresponding time intervals, having slopes that are close to the KPZ and EW behaviors,  $\beta_{\text{KPZ}} = 1/3$  and  $\beta_{\text{EW}} = 1/4$ , respectively. All units are arbitrary.

$t = 0.1$  to  $t = 3000$  for  $L = 75$ , with 200 samples and  $A_n = 3$ . For all shown cases, prior to saturation there is a scaling regime characterized by a exponent value  $\beta = 0.33 \pm 0.01$  as given by a fit for the time range indicated in the figure. The overlap of the three curves is remarkable, this scaling behavior appearing to be quite independent on parameter  $A_0$  being non-zero. Notice that equation (8) corresponds to non-equilibrium (irreversible) growth even if  $A_0 = 0$ , due to removal of self-intersections. The behavior shown in Fig. 2 provides evidence on our claim that  $A_0$  is irrelevant to the scaling behavior. We reach a similar conclusion from the measurements of additional exponents, although the results shown below will mostly consider  $A_0 \neq 0$  conditions.

Additionally, the value of  $A_1$  is seen in Fig. 2 to have little effect in the strong coupling KPZ scaling behavior. However, for smaller system sizes or smaller noise amplitudes, the observed value of the growth exponent  $\beta \simeq 0.25$  is closer to that of the Edwards-Wilkinson universality class, see the right panel in Fig. 2, suggesting the system is in a preasymptotic transient for such parameter conditions, as expected from results in the Monge gauge [37], compare both panels of our Fig. 2 with e.g. Figs. 2 and 4 in [38, 39], where accurate numerical simulations of the standard KPZ equation are reported using a pseudospectral method.

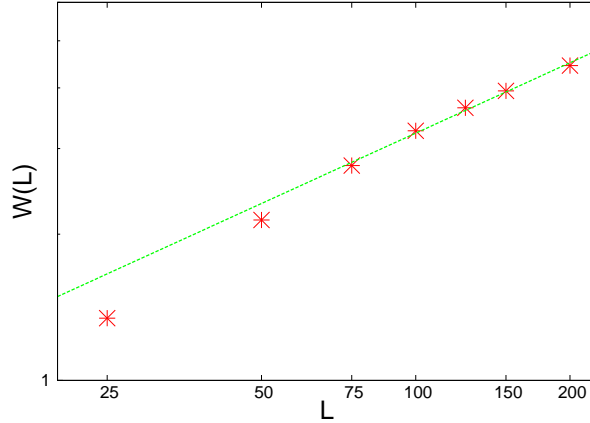


FIG. 3. Global interface width as a function of system size. For comparison, the straight line is obtained from a fit of the behavior for  $75 \leq L \leq 200$  and has a slope corresponding to  $\alpha = 0.51$ , compatible with  $\alpha_{\text{KPZ}} = 1/2$ . In all cases  $A_0 = 1$ ,  $A_1 = 0.1$ , and  $A_n = 3$ . All units are arbitrary.

Regarding the value of the roughness exponent, indeed Fig. 3 also shows the approach to an asymptotic value compatible with the KPZ universality class for sufficiently large system sizes  $L$ . Thus, the global width is plotted in this figure as a function of  $L$  for fixed  $A_0 = 1$ ,  $A_1 = 0.1$ , and  $A_n = 3$ . In the figure, we estimate  $\alpha = 0.51 \pm 0.03$  from a fit of the behavior for the largest system sizes  $75 \leq L \leq 200$ . In general, the transition from non-KPZ preasymptotic (small  $L$ ,  $A_n$  values, weak coupling regime) to asymptotic KPZ (large  $L$ ,  $A_n$  values, strong coupling regime) scaling behavior is not particularly correlated with an increasing dynamical role of self-intersection removal. The simulations show that the length of interface that is removed per unit time reaches a constant non-negligible value for generic parameter and system size conditions.

The large slopes and overhangs seen in Fig. 1 suggest a study of the statistics of the *local* angle  $\theta$  shown by the interface with respect to the *global* horizontal direction. The left panel of Fig. 4 shows the angle histogram (i.e., angle probability distribution) for  $L = 75$  and different values of the parameters, once saturation was achieved. A fit is shown to an exponential distribution of the form  $C_1 \exp(-C_2|\theta|^\chi)$ . Again,  $A_0$  does not seem to play any role in this behavior, and the three curves overlap. The right panel shows the evolution of this histogram as  $L$  increases. Fits to the same exponential form are also displayed. The corresponding values of  $\chi$  increase with  $L$ , stabilizing to a value close to 2, i.e., the distribution becomes Gaussian. In any case, the symmetric exponential distribution (as opposed to a power-law one) centered around the origin implies that the system has a

*characteristic slope* that is horizontal. Of course, the probability distribution can not be truly Gaussian, since the angle domain is bounded in  $[-\pi, \pi]$ .

The change in the *local* morphological properties for increasing size  $L$  goes beyond the angle histogram. Thus, the local roughness exponent  $\alpha_{\text{loc}}$  is close to  $1/2$  for small noise amplitudes  $A_n \leq 1$ . If the noise amplitude is large ( $A_n = 3$ ), for small systems ( $L < 50$ ) this exponent takes an effective value that can raise even above  $0.6$ , see left panel on Fig. 5 where the local interface width at saturation,  $w(l)$ , is shown as a function of the local scale, for different system sizes  $L$  and fixed  $A_0 = 1$ ,  $A_1 = 0.1$ , and  $A_n = 3$ . Moreover, the non-complete overlap of e.g. the curves for  $L = 25, 50$ , is reminiscent of anomalous scaling behavior. However, for larger values of  $L > 75$  the local roughness exponent converges to an  $L$ -independent value  $\alpha_{\text{loc}} = 0.51 \pm 0.01$ , namely, close within error bars to the  $1/2$  value it takes both for the standard EW and KPZ equations in 1D. Moreover, for these system sizes curves overlap, a fact that indicates that asymptotic scaling is not anomalous. The right panel in the same figure shows how the local width  $w(l, t)$  curves evolves with time for our largest system size,  $L = 200$ . The curves give the behavior of the local width with  $l$  for different times. Apart from times that are comparable with the discretization unit, for which no proper correlations have built up, curves for increasing times overlap in the form that again is expected for FV scaling. As time evolves, the lateral correlation length  $\xi(t)$  increases, finally reaching a steady state value at which  $\alpha_{\text{loc}} \simeq 0.5$  is obtained from a fit of the large  $l$  behavior, compatible with the value of the global roughness exponent  $\alpha$  found above.

Actually, we can employ the *local* morphological behavior just considered in order to measure the dynamic exponent  $z$ , as an alternative check to assess the asymptotic behavior of our system. As mentioned above, within the Family-Vicsek Ansatz, the saturation time  $t_s \sim L^z$ , a relation which is also fulfilled for local scales,  $t_s(l) \sim l^z$ . This implies that, if time is measured in units of  $l^z$  and the local interface width is measured in units of  $l^\alpha$ , all the  $w(l, t)$  curves should collapse. This is shown in Fig. 6 for the  $L = 200$  curves shown on the right panel of Fig. 5. As usual [1], the values of  $\alpha$  and  $z$  are chosen so that the overlap between the curves is maximum. This occurs for  $\alpha = 0.52 \pm 0.2$  and  $z = 1.4 \pm 0.1$ , again in agreement with the KPZ values for the roughness and the dynamic exponents, respectively.

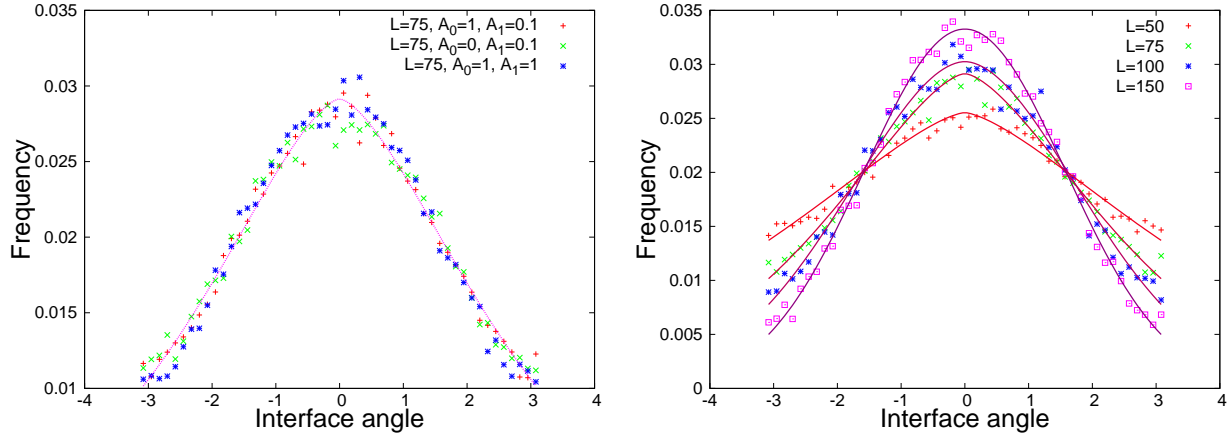


FIG. 4. Left panel: angle histograms are shown at saturation for different choices of  $A_0$  and  $A_1$ ,  $L = 75$ , and  $A_n = 3$ , obtaining very similar results. The solid line is a fit to a shape  $C_1 \exp(-C_2|\theta|^\chi)$  with  $\chi = 1.54$ . Right panel: for fixed  $A_0 = 1$ ,  $A_1 = 0.1$  and increasing size, the angle histograms can be seen to evolve towards a Gaussian profile. Solid lines are fits similar to that in the left panel with  $\chi = 1.44, 1.54, 1.84, 1.99$  for increasing  $L$ .

## VI. CONCLUSIONS AND OUTLOOK

We have characterized the scaling properties of a continuum stochastic model of one-dimensional interfaces, given by Eq. (9). The model captures the main physical mechanisms believed to characterize non-conserved, irreversible surface growth, as described in particular within the KPZ approach to non-conserved interface dynamics, namely, growth along the local normal direction with a rate that is affected by local curvature and by fluctuations in growth events, but without assumptions on small slopes or absence of overhangs. Our numerical simulations are tailored to avoid these simplifications, and lead to a number of results. In spite of the possibility for the surface to develop arbitrarily large slopes, a fact that is frequently associated with anomalous scaling, the kinetic roughening properties fulfill, rather, the Family-Vicsek Ansatz. There are predictions on the non-occurrence of non-trivial anomalous scaling at the steady state of local growth equations [40]. In principle, these predictions are done within a small slope approximation so that our present result supports their validity beyond such constraint for the specific example that we have studied. This suggests in turn the interest of assessing the corresponding situation for other continuum models beyond the small slope approximation.

Regarding the specific type of scaling that we find, for system sizes and/or noise am-



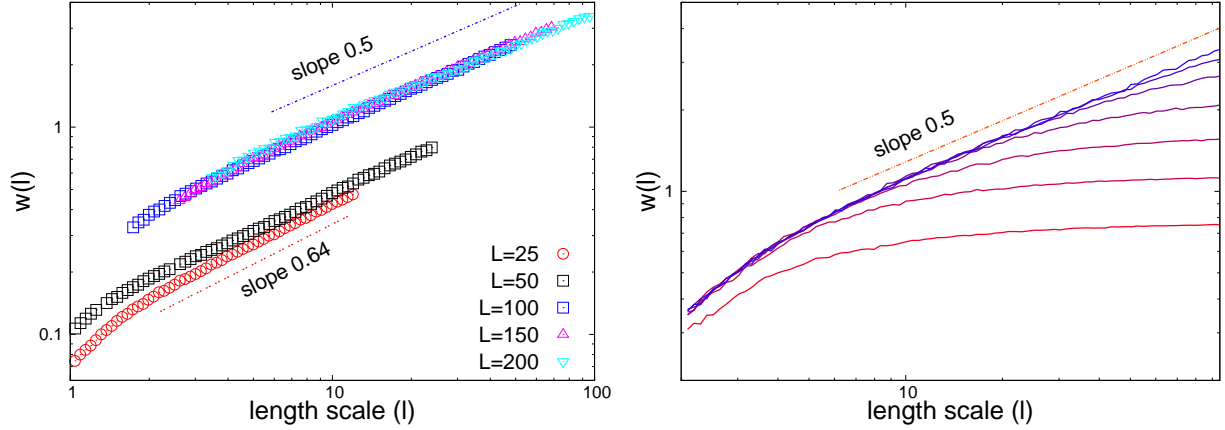


FIG. 5. Left panel: local interface width as a function of scale,  $w(l)$ , at saturation for different system sizes as indicated. In all cases,  $A_0 = 1$ ,  $A_1 = 0.1$ , and  $A_n = 3$ . The two groups of curves ( $L < 75$  and  $L > 75$ ) have been artificially offset for clarity. Notice the overlap between the different curves for  $L \geq 100$ , implying that scaling is FV. The small  $L < 100$  behavior is slightly anomalous, and characterized by a different value of  $\alpha_{\text{loc}}$ . The solid lines are obtained from fits for the smallest and largest values of  $L$  in the corresponding regions of  $l$ . Their slopes provide the value  $\alpha_{\text{loc}}$  in each case. Right panel: local interface width  $w(l, t)$  vs scale for  $L = 200$  and logarithmically equispaced times between  $t = 0.1$  and  $t = 200$ , bottom to top. The straight line with slope  $\alpha_{\text{loc}} = 0.5$  is obtained from a fit of the behavior for the top curve within the corresponding range of  $l$ . All units are arbitrary.

plitudes that are small, the system is in a preasymptotic state within which the growth exponent is close to that of the EW universality class, while the roughness exponent [41] is close to but not necessarily equals the corresponding EW value. In any case, for sufficiently large system sizes and/or noise amplitudes, Eq. (9) turns out to be in the KPZ universality class. Naturally, this result agrees with general considerations based on symmetries and conservation laws [1, 2], but we find it to be non-trivial. To the best of our knowledge, it is found for the first time for a SPDE that can access height configurations that are not constrained by the small slope and no-overhang approximations. Note moreover that, as a result of the very formulation of Eq. (9), the role of noise in this system is very far from the standard KPZ case. Thus, in the latter noise is decorrelated only in the  $x$ -axis. Adoption of that type of noise in our system would amount to assuming that all interface points which share the same  $x$ -coordinate are correlated, disregarding their distance in the vertical direction. In our case, noise is decorrelated both in the horizontal and vertical directions, as

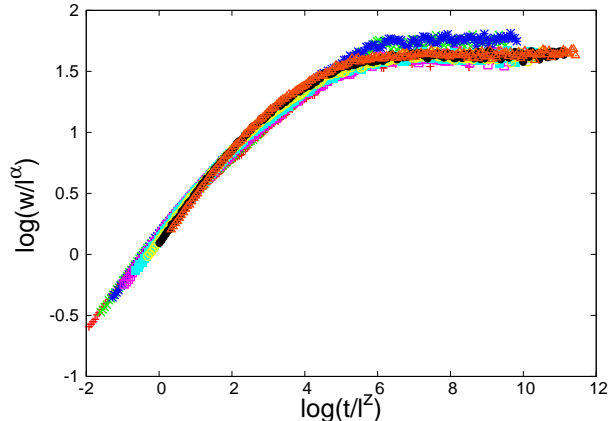


FIG. 6. Data collapse of the local interface width  $w(l, t)$  curves of the right panel on Fig. 5 ( $L = 200$ ). Collapse is achieved for  $\alpha = 0.52$  and  $z = 1.4$ . All units are arbitrary.

seen in Eq. (7). Thus, its naive spatial scaling dimension should be 2 rather than 1. Even a power counting argument [1] on the KPZ equation with this modification leads to a different result, since it provides consistent scaling exponents which differ from the KPZ universality class. Thus, our present numerical results are not evident from this point of view.

In our simulations, we have seen moreover that our extra condition on self-intersection removal plays a non-negligible role, in particular driving the system out of equilibrium even when  $A_0 = 0$ . Note that in any case the equilibrium problem associated with Eq. (9) is well understood [42]. In our case, this condition is the price we have to pay in order to have mathematically a simply-connected interface. Physically, the condition on self-intersection removal might be thought of as playing a similar simplifying role as the condition of a phantom membrane plays with respect to more realistic polymerized membranes [42]. Still, we believe the ensuing model features non-trivial physics. Perhaps this can be appreciated better if we think of still more realistic models of growth, of which Eq. (9) and similar equations are simplified versions. In those, the dynamics of the interface is coupled to that of a physical field, such as e.g. the concentration of aggregating units in the dilute phase, in what mathematically is described as a (stochastic) moving boundary problem, see e.g. [30, 43]. For parameter conditions in which kinetic roughening occurs, voids and bubbles can indeed be created (leading to a multiply connected interface), see e.g. [29], but their role for the morphological evolution seems to be quite marginal [30]. Incidentally, self-intersection removal seems to be a relevant stabilizing mechanism in face of morphological instabilities, as in ox-bow formation in meandering rivers [44, 45]. In stable-growth moving boundary

problems, the main role in the evolution is played, rather, by the envelope of the so-called active growth zone, that corresponds in our model to the simply connected interface that we keep track of after self-intersection removal. From this point of view, our choice does not seem too distant from the standard procedure by which the full interface dynamics of e.g. discrete growth models that lead to bubbles and overhangs due to e.g. bulk vacancies [46] is traded for that of its single valued approximation.

An interesting future extension of the present work is the study of the full Eq. (8), namely, for a non-zero  $A_2$  coefficient, that would allow us to study surface diffusion within the present framework, with potential implications in the context of thin film growth by MBE [10]. Given the slow dynamics associated with relaxation by surface diffusion, this would require improvements on the more computationally expensive ingredients of our adaptive numerical scheme, conspicuously including the self-intersection removal algorithm.

Moreover, given the geometrically intrinsic nature of the dynamics, the numerical approach, and the measurement techniques developed in the present work —by which nonlinearities and noise correlations, which would appear in the Monge gauge, come out naturally—, additional interesting applications would be the study of growth in a circular geometry (see a recent discussion in [26] and references therein) and the extension to two-dimensional interfaces. In both cases there are still interesting open theoretical and experimental challenges.

## ACKNOWLEDGMENTS

We would like to thank the two anonymous reviewers for their insightful remarks and recommendations, as well as Carlos Escudero for useful discussions. S. N. S. thanks the plasma physics group of Universidad Carlos III de Madrid for granting her access to their computational facilities. This work has been supported by Spanish MICINN grant No. FIS2009-12964-C05-01.

- 
- [1] A.-L. Barabási and H. E. Stanley, *Fractal concepts in surface growth* (Cambridge University Press, Cambridge, 1995).
  - [2] J. Krug, *Adv. Phys.* **46**, 139 (1997).
  - [3] J. J. Ramasco, J. M. López, and M. A. Rodríguez, *Phys. Rev. Lett.* **84**, 2199 (2000).

- [4] J. Asikainen, S. Majaniemi, M. Dubé, and T. Ala-Nissila, Phys. Rev. E **65**, 052104 (2002).
- [5] J. Asikainen, S. Majaniemi, M. Dubé, J. Heinonen, and T. Ala-Nissila, Eur. Phys. J. B **30**, 253 (2002).
- [6] G. Odor, Rev. Mod. Phys. **76**, 663 (2004).
- [7] M. Kardar, G. Parisi, and Y.-C. Zhang, Phys. Rev. Lett. **56**, 889 (1986).
- [8] J. Villain, J. Phys. I **1**, 19 (1991).
- [9] Z.-W. Lai and S. D. Sarma, Phys. Rev. Lett. **66**, 2348 (1991).
- [10] A. Pimpinelli and J. Villain, *Physics of Crystal Growth* (Cambridge University Press, Cambridge, 1998).
- [11] S. A. Safran, *Statistical thermodynamics of surfaces, interfaces, and membranes* (Addison-Wesley, Reading, MA, 1994).
- [12] M. Marsili, A. Maritan, F. Toigo, and J. R. Banavar, Rev. Mod. Phys. **68**, 963 (1996).
- [13] F. Family and J. G. Amar, Fractals **1**, 753 (1993).
- [14] A. Maritan, F. Toigo, J. Koplik, and J. R. Banavar, Phys. Rev. Lett. **69**, 3193 (1992).
- [15] R. Cuerno and L. Vázquez, in *Advances in Condensed Matter and Statistical Physics*, edited by E. Korutcheva and R. Cuerno (Nova Science Publishers, New York, 2004).
- [16] R. Cuerno, M. Castro, J. Muñoz-García, R. Gago, and L. Vázquez, Eur. Phys. J. Special Topics **146**, 427 (2007).
- [17] K. A. Takeuchi and M. Sano, Phys. Rev. Lett. **104**, 230601 (2010).
- [18] T. Sasamoto and H. Spohn, Phys. Rev. Lett. **104**, 230602 (2010).
- [19] M. Prähofer and H. Spohn, Phys. Rev. Lett. **84**, 4882 (2000).
- [20] C. Escudero, Phys. Rev. Lett. **100**, 116101 (2009).
- [21] J. Krug, Phys. Rev. Lett. **102**, 139601 (2009).
- [22] C. Escudero, Phys. Rev. Lett. **102**, 139602 (2009).
- [23] A. Brú, D. Casero, S. de Franciscis, and M. A. Herrero, Math. Comput. Model. **102**, 139602 (2008).
- [24] M. Siegert and M. Plischke, Phys. Rev. Lett. **68**, 2035 (1992).
- [25] V. G. Miranda and F. D. A. Aarão Reis, Phys. Rev. E **77**, 031134 (2008).
- [26] C. Escudero, J. Stat. Mech. , P07020 (2009).
- [27] R. Kapral, R. Livi, G.-L. Oppo, and A. Politi, Phys. Rev. E **49**, 2009 (1994).
- [28] M. T. Batchelor, B. I. Henry, and S. D. Watt, Physica A **260**, 11 (1998).

- [29] P. Kéblinski, A. Maritan, F. Toigo, R. Messier, and J. R. Banavar, Phys. Rev. E **53**, 759 (1996).
- [30] M. Nicoli, M. Castro, and R. Cuerno, J. Stat. Mech. , P02036 (2009).
- [31] W. W. Mullins, J. Appl. Phys. **28**, 333 (1957).
- [32] W. W. Mullins, J. Appl. Phys. **30**, 77 (1959).
- [33] M. Desbrun, A. N. Hirani, M. Leok, and J. E. Marsden, (2005), arXiv:math/0508341.
- [34] R. Gallego, M. Castro, and J. M. López, Phys. Rev. E **76**, 051121 (2007).
- [35] M. M. Alvarez, F. J. Muzzio, S. Cerbelli, A. Adrover, and M. Giona, Phys. Rev. Lett. **81**, 3395 (1998).
- [36] Y.-P. Zhao, G.-C. Wang, and T.-M. Lu, *Characterization of Amorphous and Crystalline Rough Surface: Principles and Applications* (Academic Press, San Diego, 2001).
- [37] E. Katzav and M. Schwartz, Phys. Rev. E **69**, 052603 (2004).
- [38] L. Giada, A. Giacometti, and M. Rossi, Phys. Rev. E **65**, 036134 (2002).
- [39] L. Giada, A. Giacometti, and M. Rossi, Phys. Rev. E **66**, 019902 (2002).
- [40] J. M. López, M. Castro, and R. Gallego, Phys. Rev. Lett. **94**, 166103 (2005).
- [41] Both, global and local roughness exponents are equal, scaling being of the FV type.
- [42] M. Plischke and B. Bergersen, *Equilibrium statistical physics* (World Scientific, Singapore, 2006).
- [43] Y. Saito, *Statistical Physics of Crystal Growth* (World Scientific, Singapore, 1996).
- [44] B. F. Edwards and D. H. Smith, Phys. Rev. E **65**, 046303 (2002).
- [45] T. B. Liverpool and S. F. Edwards, Phys. Rev. Lett. **75**, 3016 (1995).
- [46] M. Schimschak and J. Krug, Phys. Rev. B **52**, 8550 (1995).